IOPscience iopscience.iop.org

Home Search Collections Journals About Contact us My IOPscience

A structural and optical study of sputtered InP films as a function of preparation temperature

This article has been downloaded from IOPscience. Please scroll down to see the full text article.

1996 J. Phys.: Condens. Matter 8 1591

(http://iopscience.iop.org/0953-8984/8/10/028)

View the table of contents for this issue, or go to the journal homepage for more

Download details:
IP Address: 171.66.16.151
The article was downloaded on 12/05/2010 at 22:51

Please note that terms and conditions apply.

J. Phys.: Condens. Matter **8** (1996) 1591–1605. Printed in the UK

A structural and optical study of sputtered InP films as a function of preparation temperature

S H Baker†, S C Bayliss‡, S J Gurman†, N Elgun† and E A Davis†

† Department of Physics, University of Leicester, Leicester LE1 7RH, UK
‡ Department of Applied Physics, De Montfort University, The Gateway, Leicester LE1 9BH, UK

Received 26 April 1995, in final form 6 November 1995

Abstract. Approximately stoichiometric InP films have been prepared over a range of substrate temperature T_s. The structure of the deposited films has been investigated by means of transmission electron microscopy (TEM), extended x-ray absorption fine structure (EXAFS) and x-ray photoelectron spectroscopy (XPS) experiments. TEM measurements reveal that samples deposited below approximately 100 °C are amorphous while films prepared above this temperature are microcrystalline in nature. Both EXAFS and XPS measurements indicate that bond angle disorder in the atomic network decreases as T_s is raised. Changes in the optical absorption properties are observed as T_s is increased, with particularly marked changes noted over the relatively narrow temperature range 110–150 °C; the bandgap E_{04} (defined as the photon energy at which the absorption coefficient is equal to 10^4 cm^{-1}) increases from 1.1 to 1.25 eV while $n(0.5)$ (the refractive index at 0.5 eV photon energy) decreases from 3.7 to 3.3 over the above 40 °C temperature range. The changes in optical properties are correlated with the structural data.

1. Introduction

Early x-ray diffraction studies on stoichiometric (or near-stoichiometric) amorphous III–V compounds [1] showed that, as for a-Si and a-Ge, tetrahedral short-range order was retained even though the long-range order of the crystal was lost. Continuous random network (CRN) models proposed by Polk [2] for the structure of a-Si and a-Ge contain an appreciable number of odd-membered rings; it was recognised that for III–V compounds this would necessarily introduce a proportion of 'wrong' bonds i.e. bonds between like atoms. A CRN model containing only even-membered rings was introduced by Connell and Temkin [3], and it was considered that this structure might be more appropriate for the III–V materials. The adoption of such a structure would imply a high degree of chemical order. Experimentally, a range of techniques, including EXAFS, XPS and optical absorption measurements, has shown that sputtered amorphous III–V materials are generally chemically ordered; a-GaAs [4, 5] and a-GaP [6] both exhibit a high degree of chemical order. Interestingly, a-InP is found to be slightly disordered [7], although the tendency is still strongly towards chemical ordering with In–P bonds favoured. Similar results have been found for flash-evaporated a-GaAs [8], although it appears that a-GaP [8, 9] and a-InP [10] prepared by this technique may be more disordered than their sputtered counterparts. Nevertheless, electron diffraction work on such materials by Dixmier *et al* [11] points towards a structural network with even-membered rings; it is therefore considered that any partial chemical disorder is 'extrinsic'

0953-8984/96/101591+15$19.50 © 1996 IOP Publishing Ltd

and imposed by out-of-equilibrium conditions during film deposition, rather than forced on the network by topological considerations.

In addition to the possibility of partial chemical disorder, configurational disorder, i.e. bond length and bond angle vibration, should be a more general feature of the structure in amorphous III–V materials. In a-GaAs [4] and a-GaP [6], we have found that there is hardly any (or only slight) static disorder in bond length, most of the configurational disorder being associated with bond angle variation; this is usual for amorphous covalent materials. The bond angle variation has been measured from EXAFS measurements [5, 6] and shown to decrease with increasing preparation temperature; for a-GaAs [5], the sharpening of core levels, measured by XPS, was found to be consistent with the deduced values for the bond angle variation. TEM experiments have revealed that the structure of sputtered GaAs films actually changes from being solely amorphous to nanocrystalline [5, 12] at only modestly elevated deposition temperatures, although in the study by Baker *et al* [5] the nanocrystallites only occupied a relatively small volume fraction compared to that of the amorphous host matrix. Changing the amount of bond angle disorder in the amorphous network might be expected to modify the size of the bandgap and the degree of band-tailing into the gap; this should therefore lead to changes in the optical absorption spectra. Calculations by O'Reilly and Robertson [13], however, suggest that it is also important in the interpretation of absorption spectra of amorphous III–V materials to consider the effect of various defect states, such as dangling bonds and wrong bonds. Measurement of such spectra for GaAs samples sputtered over a range of temperatures [5] indicated, in the light of the work of O'Reilly and Robertson [13], that dangling bonds may be the more significant defects in this material.

The current investigation focuses on the effect on structural and optical properties of changing preparation temperature for approximately stoichiometric sputtered InP films, briefly reported on previously [14]. In particular, the changes in both chemical and configurational disorder are investigated. Structural information is obtained by means of TEM, EXAFS and XPS experiments. Optical absorption measurements are also reported and the results correlated with the structural data.

2. Preparation

Thin-film InP samples, approximately 1 μm in thickness, were sputtered from a 4 in crystalline InP target. The pressure during sputtering was about 5 mTorr and the power applied to the target 200 W at a frequency of 13.56 MHz. Prior to admitting the sputtering gas, the system was evacuated to a base pressure of 2×10^{-7} Torr. Samples were deposited at various temperatures with T_s, the temperature of the substrate during deposition, ranging between room temperature and 200 °C. T_s was measured by means of a chromel–alumel thermocouple, with an accuracy of ±5 °C or better. A variety of substrates was included in each deposition run: copper and aluminium foil for EXAFS and XPS measurements respectively, pieces of polished c-Si wafer for infrared work and Corning 7059 glass for optical absorption measurements.

In a previous study, we found that InP films sputtered from a stoichiometric InP target were slightly In rich, containing only 42 at.% P. For the current work, a few P pieces were therefore added to the target in order to deposit films with compositions nearer stoichiometry. The compositions of the samples were checked from the relative height of the P K absorption edges (as explained in subsection 4.1), and were found to lie between 48 and 56 at.% P. Table 1 gives the composition values.

Table 1. Composition of sputtered InP films determined from relative height of P K absorption edges.

T_s (°C)	In content (at.%)	P content (at.%)
36	0.45	0.55
56	0.45	0.55
85	0.44	0.56
108	0.44	0.56
156	0.49	0.51
200	0.52	0.48

3. Microstructural details

The amorphicity of the sputtered InP samples was investigated by means of transmission electron microscopy (TEM) measurements, carried out using a Jeol 100 CX instrument. The sample compositions could be checked using energy dispersive x-ray analysis (EDAX) *in situ*; all were found to lie close to stoichiometry, with composition variations across each sample of ±2 at.% or less. Further details of the TEM experiments can be found in [14]. For films deposited at 85 °C or less, the diffraction patterns consist only of a few diffuse rings, confirming the amorphicity of these samples. Furthermore, no evidence for any nanocrystals with sizes of 10 Å or more (the resolution of the TEM) was found in the corresponding real space micrographs. For substrate temperatures $T_s \geqslant 108\,^\circ$, however, sharp rings appear in the diffraction patterns, which become thinner and increasingly 'spotty' as T_s is increased. (Pictures of the electron diffraction patterns may be found in [14].) The micrograph for the sample deposited at 108 °C reveals the presence of uniformly distributed inhomogeneities, presumed to be nanocrystallites, of size 10–20 Å, which occupy a small fraction of the sample volume. As T_s is raised, the volume fraction occupied by the nanocrystallites becomes more significant and the average crystallite size increases; for $T_s = 156\,^\circ$C, at least half the sample volume is crystalline, while the average crystallite diameter is 50 Å. The diffraction patterns for the nanocrystalline samples yielded lattice spacings which correlated well (to within ±0.1 Å) with values obtained from a c-InP wafer.

4. Experimental details

4.1. EXAFS

EXAFS measurements on the sputtered InP samples were performed at the synchrotron radiation source at Daresbury Laboratory. The x-ray absorption μ was measured about the P K and In L3 edges.

Both edges occur at fairly soft x-ray energies (2.14 keV for the P K edge, 3.73 keV for the In L3 edge); EXAFS measurements for both edges were therefore carried out on station 3.4 (SOXAFS—soft x-ray absorption fine structure). The x-rays were focused by means of a Cr-plated mirror, which also provided a high-energy cut-off at about 4 keV so that harmonic contamination was minimized. A Ge(111) double-crystal monochromator defined the energy of the incident beam, while the incident intensity was measured by an Al foil [15]. Absorption at the sample was measured using the electron drain current technique [16], a variation of the total electron yield method, which measures the electron drain required to earth the sample after electron emission. Samples for EXAFS measurements were therefore deposited onto copper substrates.

The electron drain technique only samples the first 100 Å or so in from the sample surface and therefore contains no substrate contribution [16]. It is therefore possible to estimate the sample composition x ($In_{1-x}P_x$) from the relative height of the absorption edge, since the absorption $\mu(E)$ is given by

$$\mu(E) \propto (1-x)\mu_{In}(E) + x\mu_P(E)$$

where μ_{In} and μ_P are the atomic absorption coefficients of In and P respectively. The ratio of μ-values just above and just below the absorption edge yields x. Values for the atomic absorption coefficients were taken from the data of Viegele *et al* [17]. As mentioned in section 2, the sample compositions deviated only slightly from stoichiometry (see table 1).

The measured absorption spectra $\mu(E)$ were background subtracted and normalized using the standard Daresbury program EXBACK [18], which fits low-order polynomials to the smoothly varying background absorption. This yields the EXAFS spectra $\chi(E)$.

The $\chi(E)$-spectra were analysed to provide experimental values for structural parameters such as bond lengths r_j, mean-square variations in bond lengths σ_j^2 and coordination numbers N_j by fitting the experimentally measured $\chi(E)$ to calculated EXAFS functions. In these studies, calculated $\chi(E)$ were obtained using the fast curved-wave theory of Gurman *et al* [19]. This was achieved with the aid of the EXCURV92 program [18] which uses a least-squares analysis. The scattering phaseshifts were calculated within the program; complex energy-dependent potentials (Hedin–Lundqvist potentials) were used. The parameters fitted with r_j, σ_j^2, N_j and E_F, the position of the Fermi level. The amplitude reduction factor A, which allows for events which result in absorption but not EXAFS, and a parameter W_i, which can be regarded as a fine-tuning parameter to take account of any small errors in the phaseshift calculations and also instrumental broadening, were obtained from EXAFS data collected from a c-InP sample. The analysis program also includes a statistical package which gives the 95% confidence limits (i.e. the $\pm 2\sigma$ errors, where σ is the standard deviation) on the (often strongly correlated) structural parameters. Further details of the experimental setup and data-analysis procedures can be found in [18].

4.2. XPS

X-ray photoelectron spectroscopy (XPS) measurements were performed in a VG Escalab spectrometer, using Al Kα radiation. Scans were recorded over a binding energy range 0–1200 eV and calibrated using the C 1s line at 284.6 eV [14]. (All samples showed very similar (surface) C contents, with the C 1s peak appearing as a very sharp line in all cases. Hardly any binding energy shift was observed in the C 1s with changing T_s; we believe that a lack of shift is unlikely to be calibration related.) The absolute energy resolution (FWHM) of the instrument was about 1.0 eV. Although the samples were not grown *in situ*, and therefore contain some surface oxidation, they were not sputter cleaned as this causes structural rearrangement. It was, however, possible to separate the oxygenated components for the P core levels investigated since the oxides produce chemical shifts of about 4 eV. For the In levels, this was unfortunately not possible since oxygen produces much smaller shifts ($\leqslant$1 eV) for these levels. The XPS data also yielded chemical compositions; these are presented in subsection 5.2 along with the other XPS results.

4.3. Optical measurements

Infrared spectra for the sputtered InP films were recorded on a double-beam Perkin–Elmer 580B spectrophotometer, with an available wavenumber range of 4000–180 cm^{-1}. Prior

to and during data-taking, the sample compartment was thoroughly purged with dry air in order to reduce absorption due to water vapour.

Measurements at visible and near-infrared photon energies were carried out using a double-beam Perkin–Elmer 330 instrument. The absorption coefficient α and refractive index n were obtained by standard transmission and reflection techniques. Photothermal deflection spectroscopy (PDS) measurements were also carried out in order to extend the range of measurable α to lower values than could be obtained from the conventional transmission and reflection measurements.

5. Results

5.1. EXAFS

In L3 edge EXAFS spectra χ (k^3 weighted) for several of the sputtered InP films are given in figure 1, together with their associated Fourier transforms. The relatively short data range for the In edge spectra was unavoidable as the In L2 edge lies only about 200 eV above the L3 edge; for P K edge EXAFS spectra, however, the noise level was sufficiently low to allow a k-range out to around 12 Å^{-1}. The lack of second or higher shells in the Fourier transforms for samples deposited at lower T_s ($T_s \leqslant 56\,^\circ$C) is consistent with the amorphicity of these samples as found by TEM. For $T_s \geqslant 85\,^\circ$C, however, a second shell can be distinguished at around 4 Å (the second-nearest-neighbour distance in c-InP is 4.13 Å). The second shell becomes more pronounced as T_s is raised; this reflects a decrease in configurational disorder of the structural network for films grown at higher temperature, and will be discussed in more detail later.

Analysis of the measured spectra, as outlined in subsection 4.1, yielded nearest-neighbour parameters, e.g. bond lengths r and Debye–Waller factors σ^2, in agreement with those obtained by us in a recent study of a-$In_{1-x}P_x$ ($0.4 < x < 0.9$) [7]. Values for the In–P bond length and Debye–Waller factor determined from P edge EXAFS data were, within experimental error, consistent with values for the same parameters deduced from In edge measurements. At the low end of the T_s-range investigated, the heteropolar bond lengths and Debye–Waller factors were found to be 2.53–2.54 Å and 0.006–0.007 Å^2 respectively; the corresponding figures measured for a c-InP sample were 2.52–2.53 Å and 0.003–0.004 Å^2. The data indicate that both the bond length and Debye–Waller factor decrease slightly as T_s is increased, although it should be pointed out that in both cases the decrease is only of the same order as the experimental error ($\leqslant \pm 0.02$ Å for r, $\leqslant \pm 0.002$ Å^2 for σ^2). Nevertheless, a reduction in σ^2 for In–P bonds towards the value measured for the InP crystal, for which σ^2 is assumed to have only a thermal contribution, would be consistent with a reduction in static bond length disorder.

As in our previous work on a-InP [7], the sputtered films were found to be slightly chemically disordered; P edge EXAFS data yielded P–P bond lengths $r_{\mathrm{P-P}}$ close to 2.20 Å, with Debye–Waller factors $\sigma^2_{\mathrm{P-P}}$ of 0.002 Å^2. In–In bonds could not, however, be detected from the In edge measurements; attempts to fit such bonds at 3.25 Å and 3.37 Å (first-nearest-neighbour distances in metallic In) or 2.88 Å (twice the covalent radius of In) did not produce significant improvements to the fit. As we have discussed previously [7], this probably reflects a large spread in the In–In interatomic distance.

The P–In and P–P partial coordinations, $N_{\mathrm{P-In}}$ and $N_{\mathrm{P-P}}$ respectively, are given in figure 2 as functions of T_s. As T_s is increased, the degree of chemical disorder does not change until approximately 100 °; for substrate temperatures above this value, however, the decrease in $N_{\mathrm{P-P}}$ and increase in $N_{\mathrm{P-In}}$ indicate that P–P bonds start to anneal out

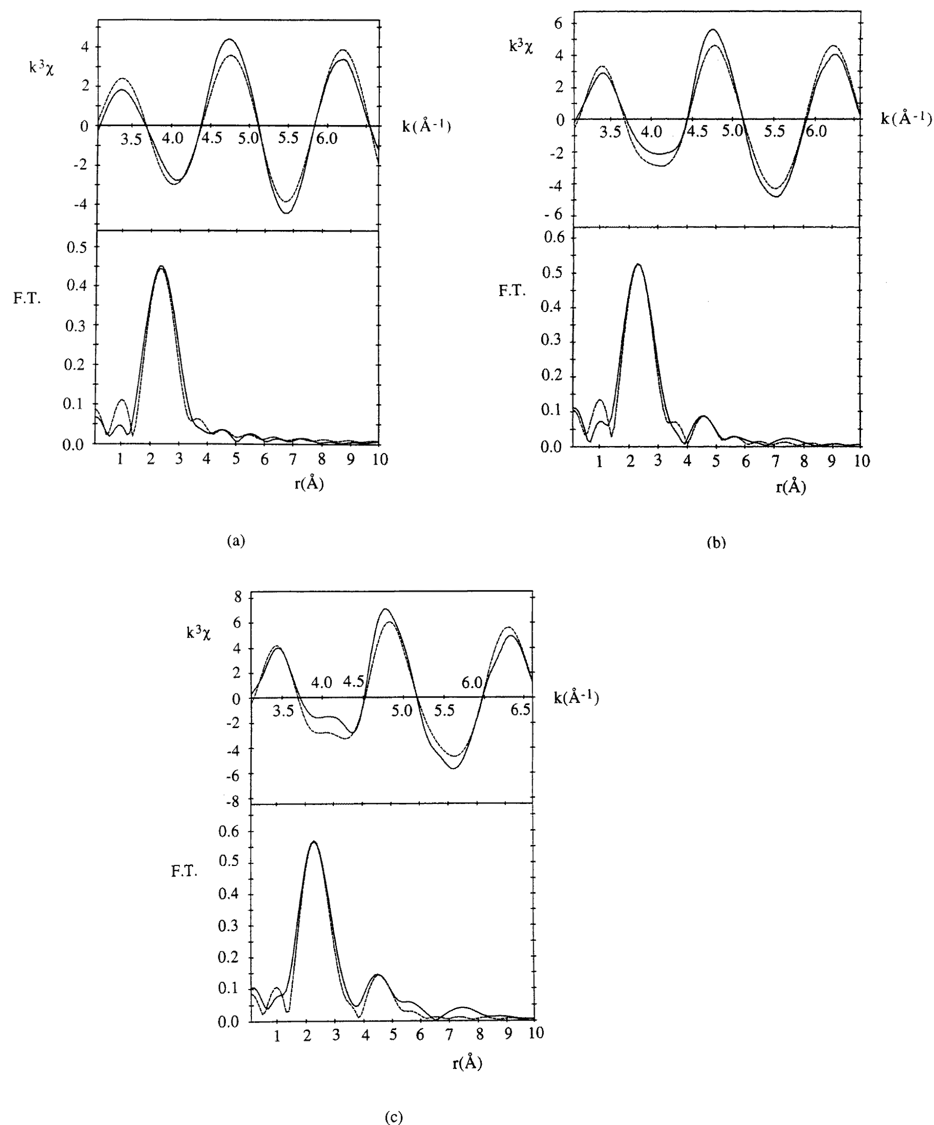

Figure 1. k^3-weighted EXAFS spectra χ and associated Fourier transforms for several sputtered InP samples: (a) $T_s = 36\,^\circ$C; (b) $T_s = 108\,^\circ$C; (c) $T_s = 200\,^\circ$C. The full lines represent the experimental data; the dashed lines give the least-squares fit.

during deposition. Films deposited above 150 °C are completely chemically ordered (within the sensitivity of the EXAFS experiments). The total P coordination N_{P-T}, obtained by summing the P partial coordinations, is consistent with four throughout the T_s-range investigated, as can be seen from figure 3 which depicts N_{P-T} as a function of T_s. Deduced, values for the In–P coordination N_{In-P}, plotted in figure 4, are consistent with the coordinations deduced from P edge data. The increase in N_{In-P} with rising T_s from values less than four at low T_s to four at higher T_s-values indicates an increase in the number of In–P bonds and hence an increase in chemical ordering; it is also consistent with our assertion that In–In bonds, although undetected in the In edge EXAFS experiments, are

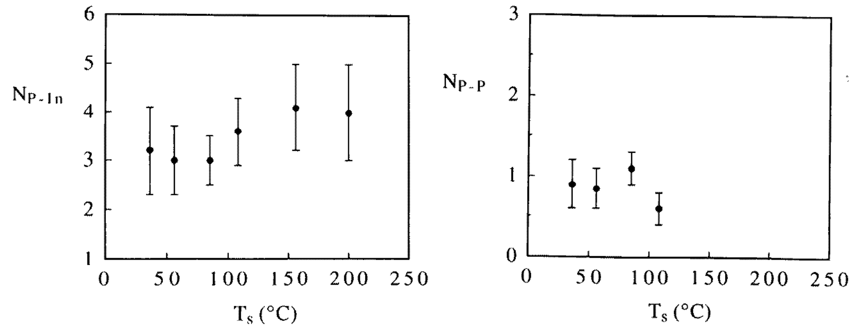

Figure 2. Partial coordinations $N_{\mathrm{P-In}}$ and $N_{\mathrm{P-P}}$ as functions of T_s.

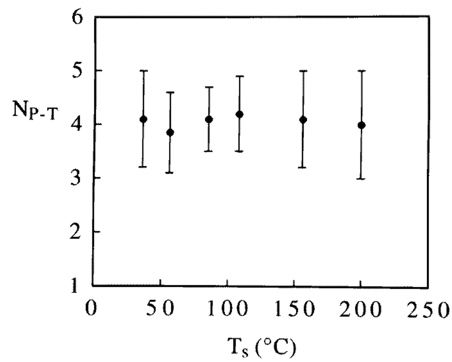

Figure 3. Total P coordination $N_{\mathrm{P-T}}$ as a function of T_s.

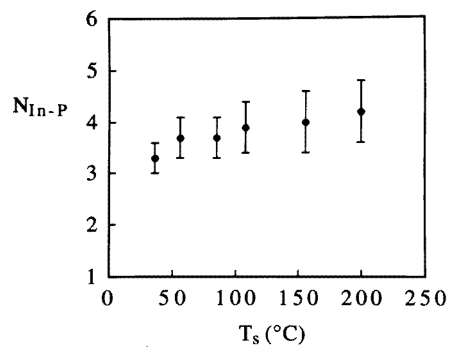

Figure 4. $N_{\mathrm{In-P}}$ as a function of T_s.

present in the films prepared at lower substrate temperatures.

Nearest-neighbour information, described above, was extracted from the experimental EXAFS spectra fairly straightforwardly. As we have already seen from figure 1, the Fourier transforms of the EXAFS spectra for samples deposited at higher T_s show small peaks corresponding to second-nearest neighbours. Fitting such small features is clearly difficult. In an effort to provide some quantitative analysis, however, the second-shell coordination was fixed at 12 (as in c-InP) while the second-shell distance r_2 and Debye–Waller factor σ_2^2

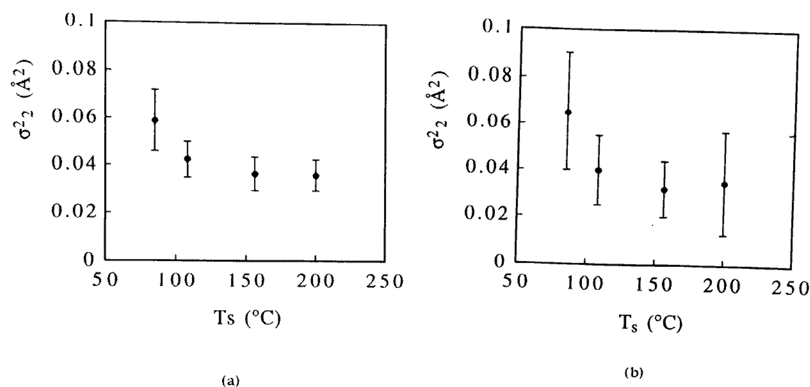

Figure 5. The second-shell Debye–Waller factor σ_s^2 as a function of T_s: (a) In edge data; (b) P edge data.

were allowed to vary freely in the fitting routine; this provided satisfactory results. Both P and In edge data yield r_2-values for the sputtered and crystal samples in the range 4.03–4.21 Å, in reasonable agreement with the value expected in c-InP of 4.13 Å, with errors of about ±0.07 Å. The deduced values of σ_2^2 are plotted in figure 5 as a function of T_s; there is no significant difference between the P and In edge results. Knowledge of the nearest-neighbour distance (r_1) and second-nearest-neighbour distance (r_2) allows the bond angle θ to be determined from simple trigonometric considerations ($2r_1 \sin(\theta/2) = r_2$). The square root of the measured Debye–Waller factors gives the root mean square variations in the bond lengths r_1 and r_2; as pointed out earlier, such variations in bond length arise from both static and thermal disorder in the case of the sputtered InP samples. With the deviations in bond lengths known (3 or 4% at most), the spread in bond angle $\Delta\theta$ may be computed using standard differential techniques. In all cases, θ was found to be close to the value expected for a tetrahedral network of about 109°. As a result of the similarity between the P and In edge σ_2^2-values (see figure 5), $\Delta\theta_{In}$ (the bond angle variation around In atoms) was found to be the same as $\Delta\theta_P$ (the bond angle variation around P atoms) for a given T_s. (It should be pointed out that $\Delta\theta_{In}$ is obtained from P edge data, while $\Delta\theta_P$ is determined from In edge measurements.) From figure 6, which gives $|\Delta\theta|$ as a function of T_s, it can be seen that $\Delta\theta$ decreases from a value too large to measure for samples deposited at low temperature to ±8° at the upper end of the T_s-range studied. For c-InP, which has only a thermal contribution to $\Delta\theta$, $\Delta\theta$ was measured at ±7°. The bond angle disorder for samples deposited above 150 °C is therefore considerably reduced relative to that for films prepared at room temperature. The similarity between $\Delta\theta_{In}$ and $\Delta\theta_P$ indicates that tetrahedral structural units with In atoms at the centre are as much distorted as P-centred ones; this is somewhat different from the situation in a-GaAs [5] and a-GaP [6] where the group V atom was found to show the greater spread in bond angle.

5.2. Core level spectra

The binding energies and FWHMs (full widths at half maximum) of P 2p and In 4d core levels were measured for the sputtered InP samples and also for a c-InP wafer. Compositions, determined from the relative areas under the peaks, are given in table 2. These values are relatively surface sensitive. Although they may be more accurate than

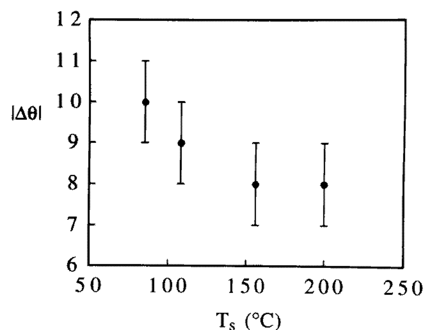

Figure 6. The magnitude of the bond angle variation $|\Delta\theta|$ as a function of T_s.

the values determined from the relative heights of the P absorption edges (at least over the depth of sample from which the data are collected), the XPS-deduced values are not necessarily more representative of the bulk composition since the EXAFS data are collected over a depth of approximately 100 Å (as mentioned in subsection 4.1)—greater than that for XPS. Furthermore, no O was detected in the P edge EXAFS; O contents of 10% or more (as found from the XPS) would be detectable if present through to a depth of 100 Å. O is therefore confined to the surface region, as expected. However, we note that the P contents and In contents determined by both techniques discussed above are similar, thereby confirming the near stoichiometry of our InP samples.

Table 2. Compositions of InP films determined from XPS. The figures in brackets denote the compositions with the In and P contents normalized to 100%, i.e. with the O content neglected; these can then be directly compared to the compositions in table 1.

T_s (°C)	In content (at.%)	P content (at.%)	O content (at.%)
56	43	45 (51)	12
85	42	44 (51)	14
108	46	44 (49)	10
156	46	46 (50)	8

Table 3. Binding energies and FWHMs of the In 4d and P 2p levels in the sputtered InP films.

T_s (°C)	In 4d binding energy (eV)	In 4d FWHM (eV)	P 2p binding energy (eV)	P 2p FWHM (eV)
56	16.9 ± 0.05	2.1 ± 0.05	127.5 ± 0.05	2.1 ± 0.05
85	16.9	2.0	127.4	2.0
108	16.9	2.0	127.3	1.8
156	17.0	1.9	127.3	1.8
c-InP	17.0	1.9	127.3	1.8

Table 3 gives the measured values of the P 2p and In 4d core level positions and FWHMs. As pointed out in subsection 4.2, oxides produce appreciable chemical shifts in the P levels, with the result that the P–O contribution was clearly resolvable from the P–In contribution

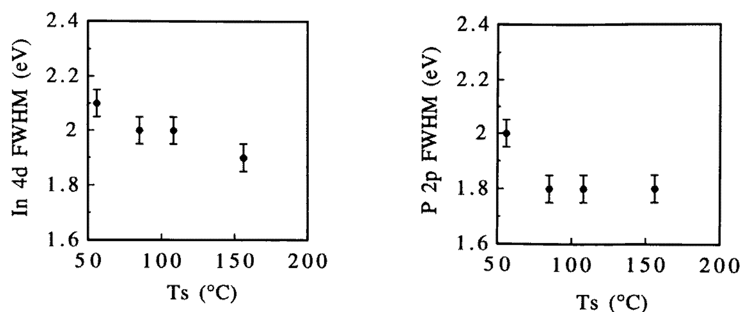

Figure 7. The FWHMs of In 4d and P 2p levels as functions of T_s. The measured In 4d and P 2p FWHMs for c-InP were 1.9 eV and 1.8 eV respectively.

in our P 2p spectra and could be separated out; hence, the P 2p binding energies documented in table 3 refer only to P–In contributions and are free from oxide effects. Although the In–O and In–P contributions to the In 4d spectra could not be resolved from each other, it was noted from the calculations of O content that most of the O is attached to P; we therefore tentatively suggest that the In 4d data are also affected little by oxide effects. For the film prepared at 56 °C, a shift of 0.2 ± 0.05 eV was found for the P 2p binding energy (relative to that measured for c-InP). The magnitude of the shift decreased gradually as T_s was increased. Despite the fact that the changes in edge shift are small (only just larger than experimental error), such a decrease would be consistent with an improvement in chemical ordering, since the P 2p level in phosphorus is approximately 2.5 eV above that in c-InP [20]; such behaviour would therefore be in agreement with the P edge EXAFS data (see figure 2). Analogous behaviour was observed for the In 4d levels, taking account of the fact that In levels in metallic In are below those in c-InP. (The In 3d levels showed similar trends in binding energy and FWHM to those found for the 4d levels.) Indications from XPS measurements of (partial) chemical disorder in a-InP have also come from Ouchene *et al* [10] and Theye *et al* [21] for flash-evaporated material, as well as from our earlier study of sputtered InP [7]. It should be noted, however, that Shevchik *et al* [22], who investigated core levels in a range of amorphous III–V compounds (prepared by d.c. sputtering), found no evidence for any core level shifts in a-InP.

The FWHM is governed not only by the instrumental linewidth and by the lifetime broadening but also by the spread in bond angle (i.e. contribution from second-nearest neighbours). For both P 2p and In 4d levels, the FWHM was found to decrease monotonically with increasing T_s towards the value measured for the c-InP wafer; figure 7 shows the FWHM for both levels. Such behaviour implies a monotonic decrease in bond angle disorder and is therefore in qualitative agreement with the EXAFS results (see figure 6).

The expected broadening of the core levels can be estimated by considering the effect on the lattice potential of varying bond angle disorder [14]. Assuming a purely Coulombic interaction, a broadening ΔE (measured in electron volts) of

$$\Delta E = 14.4q\left(r_1^{-1} - r_2^{-1}\right)$$

may be expected, where q (measured in units of e) is the charge transferred as a result of the ionicity of the material and r_1 and r_2 are the minimum and maximum distances (measured in ångströms) from the outer core levels to the second-nearest neighbours for a given bond

angle disorder (determined from the EXAFS measurements). q can be estimated from the Phillips ionicity (following Shevchik *et al* [22]) and is about 0.7 e. For the In 4d levels, the above model suggests that ΔE varies uniformly from 0.6 eV for $T_s = 56\,^{\circ}$C (assuming $\Delta\theta = \pm 10^{\circ}$) to 0.4 eV for c-InP. The changes in this term are consistent within error with the measured changes in FWHM. Similar changes in ΔE were found for the P levels. Note that the values of the lattice term ΔE are larger than those found for GaAs [5] because of the increased charge transfer. However, since bond angle disorder and distances vary at a smaller rate for those materials as T_s is increased, the variations in this term are also similar. It should be pointed out that the approach described above is a simplification of the situation. A more complete picture takes account of the fact that the potential seen by core electrons can be divided into three parts: (i) the potential due to core charges and nearest neighbours, (ii) a bonding charge and (iii) the lattice contribution. However, if there are few wrong bonds, the term expected to vary most is the Coulombic lattice contribution, since the bonding and core charge terms will be approximately the same on average even if the bond angle disorder changes.

In addition to the core levels, the plasmon energies E_P could also be obtained from the measured XPS spectra. E_P for the In 4d levels was found to increase monotonically from 14.5 ± 0.1+eV for $T_s = 56\,^{\circ}$C to 14.8 ± 0.1 eV for c-InP. Hence, since E_P is given by

$$E_P = \left\{ \frac{Ne^2}{\varepsilon_0 m} \right\}^{1/2}$$

where m is the electron mass, the charge density N and therefore the atomic density also increase monotonically with rising T_s [14]. We shall return to this point in section 6.

5.3. Infrared data

Figure 8 gives infrared transmission spectra for several of the InP samples. In each case, a strong absorption mode in the vicinity of 300 cm^{-1} is observed; this feature corresponds to the In–P TO (transverse optic) mode, which is a bond stretch. For $T_s \leqslant 56\,^{\circ}$C, the TO mode is broad and centred at approximately 280 cm^{-1}, in agreement with recent results [7]. In the case of the sample deposited at 85 °C, a slight shift in the position of the TO mode to about 300 cm^{-1} is observed. Considerable sharpening and a shift to the position associated with c-InP of 305 cm^{-1} occurs for samples prepared at still higher temperature ($T_s \geqslant 108\,^{\circ}$C). The wavenumber shift and sharpening of the TO mode reflect the decrease in configurational (mostly bond angle) disorder of the amorphous network as T_s is raised and also the increasing microcrystallinity of the samples.

5.4. Optical absorption edge

Figure 9 gives the optical absorption coefficient α as a function of photon energy $\hbar\omega$ for several of the sputteed InP films; data from the transmission and reflection experiments are combined with those from PDS in the absorption curves. The position and also the width of the absorption edge clearly shift to higher energy with increasing T_s.

Bandgaps E_T were determined from the absorption data using the Tauc relation [23]

$$(\alpha\hbar\omega) = B\left(\hbar\omega - E_T\right)^2.$$

E_{04}, the photon energy at which $\alpha = 10^4$ cm^{-1}, was also used as a measure of the bandgap. Both E_T and E_{04} are plotted as functions of T_s in figure 10. For the lowest T_s-value, investigated here (36 °C), the measured bandgap is in good agreement with that found by

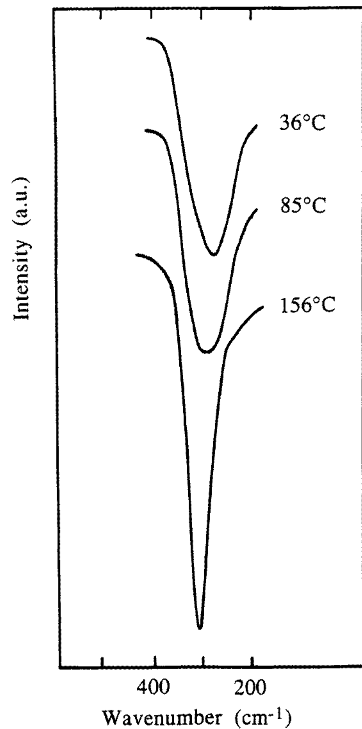

Figure 8. Infrared transmission spectra for several of the sputtered InP samples. The substrate temperatures label the spectra.

us [7] and others [24] for a-InP deposited at room temperature. (The bandgap in c-InP is approximately 1.4 eV.) The most striking feature in figure 10 is the sharp increase in E_T and E_{04} between approximately 110 °C and 150 °C, although it should be noted that there is a slight increase in bandgap with increasing T_s for $T_s \leqslant 110$ °C. This behaviour is somewhat different to that found by us [5] for sputtered GaAs, for which the bandgap increased uniformly with increasing T_s. (The slight decrease in bandgap for the InP sample deposited at 200 °C may be attributed to the fact that this film is slightly In rich—the only such sample in this study.)

Other optical properties of the InP samples also show sharp changes between approximately 110 and 150 °C. From figure 11, it is clear that there is a marked drop in the refractive index at this point. For α-values of 10^4 cm^{-1} or less, the absorption edges are exponential in form and can be fitted by

$$\alpha = \alpha_0 \exp\{\hbar\omega/E_U\}$$

where α_0 and E_U are constants. Such behaviour is common in amorphous semiconductors; the exponential edge is often referred to as the Urbach edge and hence E_U is sometimes known as the Urbach edge parameter. At low T_s-values, E_U is approximately 90 meV and agrees closely with figures measured by us [7] previously for stoichiometric material prepared at room temperature. Above 110 °C, a clear increase in E_U to about 200 meV reflects distinct broadening of the absorption edges at this point.

The trends in optical properties described above are discussed in the following section, not only in relation to the other data presented in this study but also with reference to the

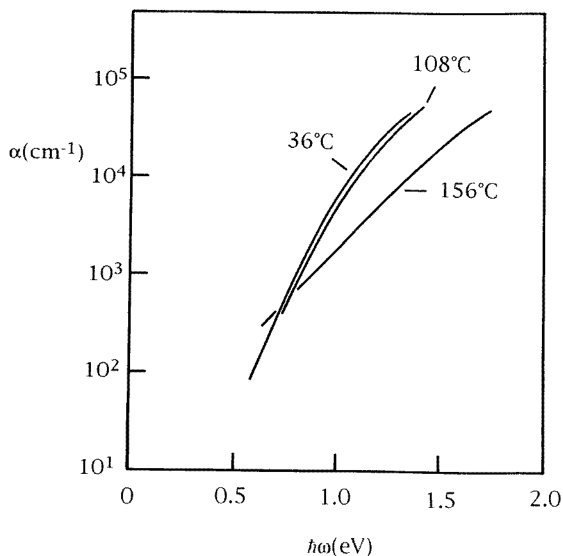

Figure 9. Examples of absorption edge spectra for the InP films. The substrate temperatures label the spectra.

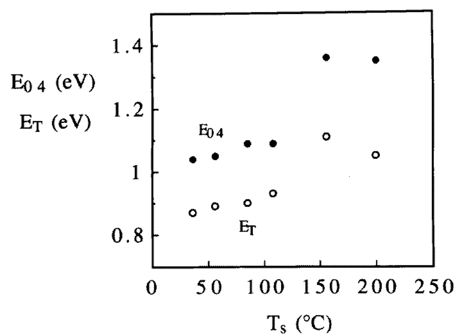

Figure 10. Bandgap, as defined by E_T and E_{04}, as a function of T_s.

work of O'Reilly and Robertson [13] who have calculated the electronic states of bulk and defect sites in amorphous III–V compounds using tight-binding recursion methods. Similar approaches have proved fruitful in previous studies on GaAs [5] and $In_{1-x}P_x$ [7] (variable x).

6. Discussion

The EXAFS and XPS results, presented in subsections 5.1 and 5.2 respectively, reveal that bond angle disorder in the InP samples decreases monotonically as T_s is raised. The disappearance of P–P bonds between 100 and 150 °C (see figure 2) suggests that the onset of crystallization (over this temperature range) occurs primarily through an increase in chemical ordering rather than a decrease in bond angle disorder. As we saw in subsection 5.4, various optical properties of the InP films such as bandgap and refractive index undergo a sharp

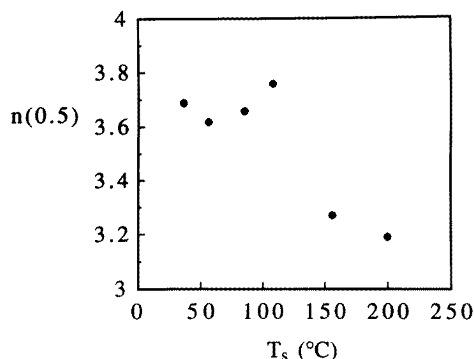

Figure 11. Refractive index (at a photon energy of 0.5 eV) as a function of T_s.

change over the same range of substrate temperature; such behaviour therefore correlates better with the onset of crystallization than the decreasing spread in bond angle $\Delta\theta$, which falls fairly uniformly with increasing T_s. In fact, calculations by O'Reilly and Robertson [13] indicate that the band edges in amorphous III–V compounds should be very little affected by bond angle disorder. (It should also be noted that from the measured plasmon energies (subsection 5.2), it was inferred that the atomic density increases fairly uniformly as T_s is raised; the sharp changes in optical properties therefore cannot be solely due to density changes as crystallization proceeds.)

O'Reilly and Robertson [13] have predicted that the energy levels associated with dangling bond defect states lie close to the band edges; cation dangling bonds are expected to produce states at or above the conduction band edge while anion dangling bonds are predicted to give states at or below the valence band edge. The gradual increase in bandgap before the onset of crystallization (see figure 10) is therefore consistent with a slowly decreasing dangling bond density in the a-InP network as T_s is raised. The appearance of crystallites in the amorphous network might reasonably be expected to lead to an increase in the density of dangling bonds, at the interfaces between the phases for example. According to the results of O'Reilly and Robertson [13], this would initially keep the bandgap low (as in our InP sample deposited at $T_s = 108\,^\circ$C, the lowest value of T_s for which crystallites were observed). An increase in bandgap would be expected when the average crystallite size becomes large enough that the dangling bond density is substantially reduced. Our data imply that this occurs over a narrow temperature range in InP, in contrast to the behaviour observed by us for GaAs [5] for which the average crystallite size was found to increase more gradually as T_s was raised. It should be pointed out that O'Reilly and Robertsons' calculations [13] indicate that P–P 'wrong' bonds result in states near the conduction band edge; the increase in chemical ordering during crystallization will therefore also contribute to an increase in bandgap. Residual numbers of wrong bond defects (far too few to be detected by the EXAFS experiments) will remain after the onset of crystallization, and may be much less inclined to anneal out during deposition than dangling bond defects. If so, this could account for the apparent broadening of the absorption edge above $T_s = 150\,^\circ$C since In–In bonds are predicted to give states near midgap. Similar absorption results have been presented by Theye *et al* [21] who found that annealing flash-evaporated InP to 200 °C had much less effect on midgap states than states nearer the band edge.

7. Conclusions

Sputtered InP films deposited at temperatures of less than approximately 100 °C are amorphous and slightly chemically disordered, in agreement with our previous work [7]. The structural network for films deposited above about 100 °C contains crystallites and shows an enhanced degree of chemical ordering. As the substrate temperature is increased, the sputtered films become increasingly microcrystalline in nature. Various optical properties of the InP samples undergo a sharp change between approximately 110 °C and 150 °C; the bandgap (E_{04}) increases from 1.1 eV to 1.25 eV with increasing T_s while the refractive index $n(0.5)$ decreases from 3.7 to 3.3. This behaviour correlates with the onset of crystallization.

Acknowledgments

The authors are grateful to J S Bates and R Bradley (Loughborough University of Technology, Loughborough, UK) for their assistance with TEM and XPS measurements respectively.

References

[1] Shevchik N J and Paul W 1974 *J. Non-Cryst. Solids* **13** 1
[2] Polk D E 1971 *J. Non-Cryst. Solids* **5** 365
[3] Connell G A N and Temkin R J 1974 *Phys. Rev.* B **9** 5323
[4] Baker S H, Manssor M I, Gurman S J, Bayliss S C and Davis E A 1992 *J. Non-Cryst. Solids* **144** 63
[5] Baker S H, Bayliss S C, Gurman S J, Elgun N, Bates J S and Davis E A 1993 *J. Phys.: Condens. Matter* **5** 519
[6] Elgun N, Gurman S J and Davis E A 1992 *J. Phys.: Condens. Matter* **4** 7759
[7] Baker S H, Bayliss S C, Gurman S J, Elgun N, Williams B T and Davis E A 1994 *J. Non-Cryst. Solids* **169** 111
[8] Theye M L, Gheorghiu A and Launois H 1980 *J. Phys. C: Solid State Phys.* **13** 6569
[9] Udron D, Flank A M, Gheorghiu A, Lagarde P and Theye M L 1989 *Phil. Mag. Lett.* **59** 9
[10] Ouchene M, Senemaud C, Belin E, Gheorghiu A and Theye M L 1983 *J. Non-Cryst. Solids* **59 & 60** 625
[11] Dixmier J, Gheorghiu A and Theye M L 1984 *J. Phys. C: Solid State Phys.* **17** 2271
[12] Murri R, Gozzo F, Pinto N, Schiavulli L, De Blasi C and Manno D 1992 *J. Non-Cryst. Solids* **127** 12
[13] O'Reilly E P and Robertson J 1986 *Phys. Rev.* B **34** 8684
[14] Bayliss S C, Baker S H, Bates J S, Gurman S J, Bradley R and Davis E A 1993 *J. Non-Cryst. Solids* **164–166** 143
[15] MacDowell A A, West J B, Greaves G N and Van der Laan G 1988 *Rev. Sci. Instrum.* **59** 843
[16] Elam W T, Kirkland J P, Neiser R A and Wolf P D 1988 *Phys. Rev.* B **38** 26
[17] Viegele W J 1973 *At. Data* **5** 51
[18] Morrell C, Campbell J C, Diakun G P, Dobson B R, Greaves G N and Hasnain S S *EXAFS Users' Manual* (Daresbury: SERC)
[19] Gurman S J, Binsted N and Ross I 1984 *J. Phys. C: Solid State Phys.* **17** 143
[20] Wagner C D 1983 *Practical Surface Analysis by Auger and X-Ray Photoelectron Spectroscopy* ed D Briggs and M P Seah (New York: Wiley) ch 4
[21] Theye M L, Gheorghiu A, Udron D, Senemaud C, Belin E, Von Bardelben J, Squelard S and Dupin J 1987 *J. Non-Cryst. Solids* **97 & 98** 1107
[22] Shevchik N J, Tejeda J and Cardona M 1974 *Phys. Rev.* B **9** 2627
[23] Tauc J 1970 *The Optical Properties of Solids* ed F Abeles (Amsterdam: North-Holland) p 277
[24] Gheorghiu A, Ouchene M, Rappeneau T and Theye M L 1983 *J. Non-Cryst. Solids* **59 & 60** 621